

## Differential elastic electron scattering by pentane

Kamil Fedus,<sup>1</sup> C. Navarro,<sup>2</sup> L. R. Hargreaves,<sup>2</sup> M. A. Khakoo,<sup>2</sup> Alessandra Souza Barbosa,<sup>3</sup> and M. H. F. Bettega<sup>3</sup>

<sup>1</sup>*Institute of Physics, Faculty of Physics, Astronomy and Informatics, Nicolaus Copernicus University, Grudziadzka 5, 87-100 Torun, Poland, EU*

<sup>2</sup>*Department of Physics, California State University, Fullerton, California 92834, USA*

<sup>3</sup>*Departamento de Física, Universidade Federal do Paraná, Caixa Postal 19044, 81531-990 Curitiba, Paraná, Brazil*

(Received 24 February 2015; published 1 April 2015)

We report measurements and calculations of the differential cross sections for elastic scattering of low-energy electrons by pentane,  $C_5H_{12}$ . The incident energies measured are at 1, 1.5, 2, 3, 5, 10, 15, 20, 30, 50, and 100 eV, and the calculations covered energies up to 100 eV. The range of experimental scattering angles is from  $5^\circ$  to  $130^\circ$ . We compare our experimental and theoretical values to each other and to available experimental and theoretical data for linear  $n$ -alkanes.

DOI: [10.1103/PhysRevA.91.042701](https://doi.org/10.1103/PhysRevA.91.042701)

PACS number(s): 34.80.Bm

### I. INTRODUCTION

Next to the molecule  $n$ -butane ( $nC_4H_{10}$ , with a research octane number of 94),  $n$ -pentane ( $nC_5H_{12}$ , with a research octane number of 62) is the simplest liquid hydrocarbon (at room temperature) contained in gasoline engines and is a major constituent of liquefied petroleum gas (LPG), an important alternative fuel for automobiles [1,2]. Ignition and reaction chemistry involving excitation, dissociation, and ionization of these molecules in combustion (plasma) processes in automobile engines [3] is governed or catalyzed by energetic electron scattering from these fuel species in the energy region which ranges from 0.1 eV to high energies ( $>100$  eV), but with a maximum around 10 eV [4]. Whereas there exist electron impact data on methane [5–7], ethane [8,9], propane [10–12], and butane [13], and in references cited within these, there is lack of electron collision data for pentane. The few data available for pentane are those by Freeman *et al.* [14] of total electron cross sections determined from the mobility of electrons in liquid pentane at the energies of 0.1 to 0.5 eV using a time-of-flight method and those by Kimura *et al.* [15] of gaseous pentane of total cross sections for this target. Floriano *et al.* [16] also reported momentum-transfer cross sections (MTCS) for gaseous pentane in the region of Ramsauer-Townsend (RT) minimum from swarm-type experiments.

Electron scattering studies of larger polyatomic molecules have received impetus since the discovery by Boudaïffa *et al.* [17] that low-energy secondary electrons were able to dissociate DNA molecules via dissociative electron attachment (DEA), which is a resonant process. This has important biological implications concerning electron impact processes on organic molecules. Whereas much work has been carried out on those molecules that make up the DNA bases or its backbone sugar, significantly less work, of a similar nature, is available on the role of electrons on hydrocarbon fuels, especially in the vapor phase (obtained from a room temperature volatile liquid) which would be used in automotive systems for both regular and diesel engines, and where combustion in engines is initiated by electrons from a spark plug or produced by compression of the gas to high temperatures to produce free electrons. One can expect DEA processes to similarly take place in these environments and to have a significant effect on the efficiency of combustion processes. In this paper we present an effort to cover this gap with pentane which is a

liquid at room temperature as compared to propane or butane, which have been investigated in the past.

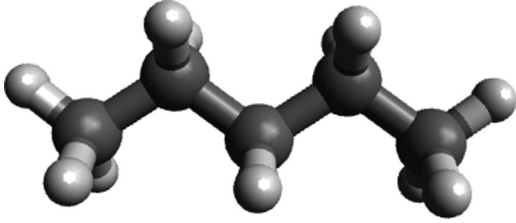
The present measurements of differential cross sections (DCSs) for elastic electron scattering from pentane were taken at incident electron energies ( $E_0$ ) of 1–100 eV for scattering angles ( $\theta$ ) of  $5^\circ$  to  $130^\circ$  using our low-intermediate energy electron spectrometer [18]. Our calculations were carried out using the Schwinger multichannel (SMC) method [19,20] with pseudopotentials [21] and were carried out in the static-exchange (SE) and static-exchange plus polarization (SEP) approximations. In addition, we compare our DCSs with similar SEP calculations for  $n$ -pentanol,  $C_5H_{11}OH$ , which is close in structure to pentane, but has a significantly larger dipole moment. At energies significantly above the ionization potential of pentane at 10.37 eV [22], we employ the SMC method in the SE approximation. A ball-and-stick model of pentane is shown in Fig. 1 which illustrates its chainlike structure and gives the positioning of C-C bonds and C-H bonds and shows how its dipole moment would be small.

The remainder of this manuscript is as follows. In Sec. II A we present our experimental procedures and in Sec. II B our theoretical method and the computational procedures employed in the present calculations. Our results and discussions are presented in Sec. III. We end the paper with a short Conclusion about our findings.

### II. METHOD

#### A. Experiment

Our experimental apparatus, which has been well tested, is detailed in our previous papers, e.g., Khakoo *et al.* [18], so only a short a summary of it is given here. The electron gun and electron analyzer had double hemispherical energy selectors to provide well-defined electron beam energy profiles. The apparatus was made of titanium cylindrical lenses with molybdenum apertures. The system was baked at a temperature of about  $130^\circ\text{C}$  using biaxial heaters [23] which did not add any significant magnetic field to our system when operated. Electrons were detected by a discrete dynode electron multiplier [24], which had a dark count rate of  $<0.01$  Hz and which was capable of linearly detecting  $>10^5$  Hz of electrons without saturating. The remnant magnetic field in the collision region area was reduced to  $\approx 1$  mG at the collision region

FIG. 1. Stick-and-ball model of pentane ( $C_5H_{12}$ ).

by a double  $\mu$ -metal shield, coupled with a Helmholtz coil that eliminated the vertical component of the Earth's magnetic field. Typical electron currents ranged around 18–28 nA, with a corresponding energy resolution of between 40 and 50 meV, full width at half maximum. Lower currents were chosen for lower  $E_0$  values in order to curtail the effects of space-charge broadening of the incident electron beam, whereas higher currents were employed at our higher energies to obtain better statistics at larger scattering angles. The electron beam varied less than 10% at maximum during the day's data acquisition. The energy of the beam was established, at least daily, by measuring the minimum in elastic scattering of the  $2^2S$  He resonance at  $E_0 = 19.366$  eV [25] at  $\theta = 90^\circ$  to better than  $\approx 30$  meV stability during an experimental run (1 day). Typically the contact potential varied from 0.6 to 0.7 eV. Energy loss spectra of the elastic peak were collected at fixed  $E_0$  values and  $\theta$  by repetitive, multichannel-scaling techniques. The effusive target gas beam was formed by flowing gas through a  $\approx 0.3$ -mm-diameter aperture mounted at the end of a  $\frac{1}{4}$ -in. aluminum tube. The whole source was sooted (using an acetylene flame) to reduce secondary electrons. The use of an aperture instead of a tube gas collimator removes the need to maintain the gas pressures of the target gases in an inverse ratio of their molecular diameters, removing a major systematic source of error that occurs in using tube collimators or similar; see, e.g., [26]. The aperture source was located  $\approx 5$  mm below the axis of the electron beam, and the source was movable in and out of alignment with the electron beam. This movable gas source arrangement [27] enabled us to expediently and accurately determine background electron-gas scattering rates. The measured DCSs were normalized using the well-known relative flow method with helium as the reference gas, using DCSs from the well-established work of Nesbet [28] for  $E_0 < 20$  eV and of Register *et al.* [29] for  $E_0 \geq 20$  eV. The pressures behind the aperture ranged from 1.2 to 2.5 Torr for He and 0.065 to 0.1 Torr for pentane, resulting in a chamber pressure ranging from  $1.0 \times 10^{-6}$  Torr to  $2 \times 10^{-6}$  Torr. Each DCS was taken a minimum of two times to check its reproducibility and a weighted average was made of multiple data sets to obtain the final DCSs. Integral cross sections (ICS) and MTCS were evaluated from the measured DCS by extrapolating the DCS to  $0^\circ$  and  $180^\circ$  and applying the standard integral formula. Each DCS set was extrapolated to  $\theta = 0^\circ$  and  $180^\circ$  by a polynomial curve which is described in [30].

### B. Theory and computational details

Our calculations were carried out using the SMC method with pseudopotentials (SMCPP) [21]. The details of the

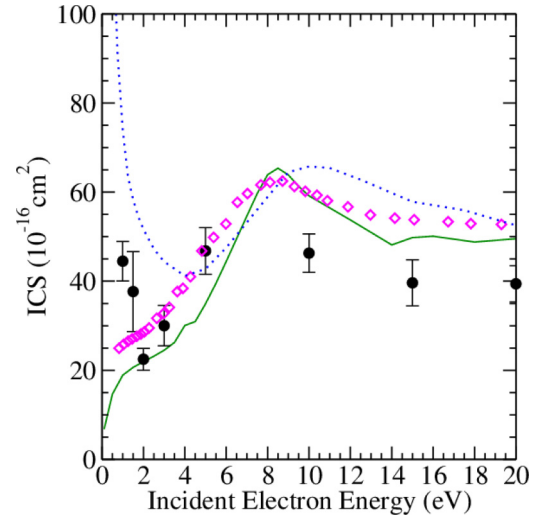


FIG. 2. (Color online) Integral cross section (ICS) for elastic scattering of electrons by pentane, in the static-exchange plus polarization approximation (—) and experimental elastic ICS (●) for pentane. We compare our results with experimental total cross section (TCS) (◇) from [15] and calculated data for  $n$ -pentanol (⋯) obtained with the SMCPP method [37].

method are not the main purpose of this work, and we will provide only the relevant points for the present calculations. The SMC method is a variational approximation to the scattering amplitude,  $f_{\text{SMC}}(\vec{k}_f, \vec{k}_i)$ , with  $\vec{k}_f, \vec{k}_i$  being the scattered and incident electron momenta. The expression for the scattering amplitude in the body frame is given by

$$f_{\text{SMC}}(\vec{k}_f, \vec{k}_i) = \frac{1}{2\pi} \sum_{m,n} \langle S_{\vec{k}_f}^- | V | \chi_m \rangle (d^{-1})_{mn} \langle \chi_m | V | S_{\vec{k}_i}^- \rangle, \quad (1)$$

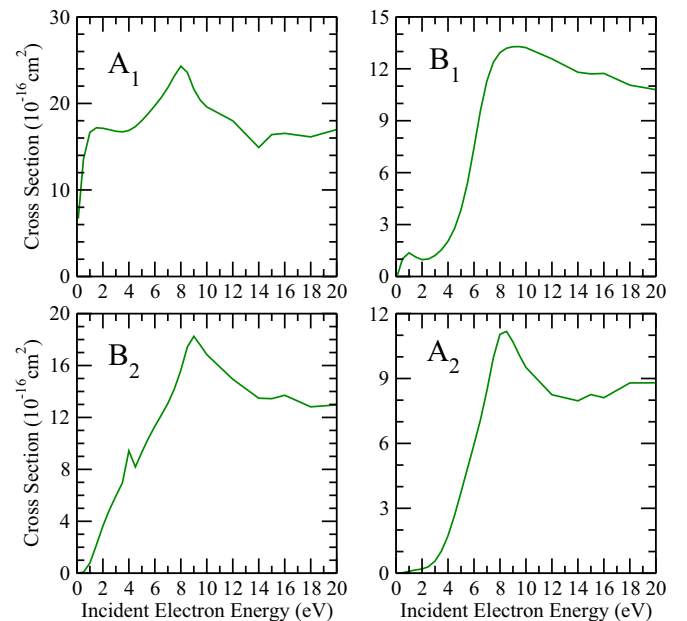


FIG. 3. (Color online) Symmetry decomposition according to the  $C_{2v}$  point group of the ICS for elastic scattering of electrons by pentane. See text.

TABLE I. Experimental DCSs ( $10^{-16} \text{ cm}^2/\text{sr}$ ), ICSs, and MTCs ( $10^{-16} \text{ cm}^2$ ) for elastic electron scattering from pentane. Error bars (1 standard deviation) include uncertainties in helium elastic DCSs (5%–8%), uncertainties in flow rates (3%–5%), statistical uncertainties (1%–5%), and standard deviation uncertainties of multiple DCSs measurements (2%–5%).

		$E_0$ (eV)										
Angle (deg)	1 eV	Error	1.5 eV	Error	2 eV	Error	3 eV	Error	5 eV	Error		
15									25.6	2.1		
20							7.01	0.64	16.1	1.3		
25			6.54	0.53	2.74	0.29	4.55	0.41	10.3	0.9		
30	1.59	0.14	3.69	0.29	1.83	0.15	2.99	0.25	6.38	0.52		
40	1.38	0.16	1.49	0.12	1.56	0.17	2.30	0.20	3.78	0.31		
50	1.71	0.15	1.29	0.10	2.02	0.18	2.53	0.22	3.62	0.30		
60	2.14	0.20	1.81	0.14	2.21	0.19	2.59	0.21	3.38	0.28		
70	2.80	0.25	2.20	0.17	2.18	0.21	2.50	0.22	3.08	0.27		
80	2.93	0.26	2.23	0.17	2.19	0.21	2.15	0.18	2.51	0.24		
90	3.20	0.27	2.40	0.19	1.85	0.17	1.79	0.15	1.94	0.17		
100	3.66	0.35	2.07	0.16	1.44	0.13	1.44	0.12	1.73	0.15		
110	4.26	0.38	1.91	0.15	1.32	0.13	1.27	0.10	1.77	0.15		
120	5.00	0.60	2.20	0.19	1.23	0.11	1.24	0.11	1.95	0.16		
125			3.83	0.34			1.27	0.12				
129			4.65	0.83								
130	5.49	0.53			1.16	0.12	1.40	0.14	2.21	0.18		
ICS	44.5	4.44	37.7	9.0	22.5	2.4	30.0	4.5	46.8	5.2		
MTCS	54.8	5.1	36.3	9.9	18.4	2.2	24.7	4.8	30.8	3.4		

		$E_0$ (eV)											
Angle (deg)	10 eV	Error	15 eV	Error	20 eV	Error	30 eV	Error	50 eV	Error	100 eV	Error	
5											113	10	
10	45.1	4.3			69.5	5.9	78.0	6.7	66.5	5.6	25.4	2.2	
15	26.8	2.3	27.4	2.8	35.3	3.1	28.8	2.4	19.7	1.7	6.84	0.59	
20	17.0	1.5	16.2	1.4	17.6	1.5	12.3	1.0	6.78	0.58	2.76	0.24	
25	10.5	0.9	9.84	0.85	8.54	0.70	6.25	0.53	3.30	0.28	1.87	0.19	
30	6.79	0.61	6.44	0.57	5.68	0.47	4.01	0.34	2.05	0.18	1.32	0.11	
40	4.15	0.36	4.18	0.37	3.27	0.27	2.25	0.19	1.38	0.12	0.597	0.052	
50	3.48	0.29	2.92	0.25	2.25	0.19	1.67	0.14	0.854	0.072	0.414	0.045	
60	2.82	0.22	2.14	0.19	1.72	0.14	1.14	0.09	0.455	0.053	0.311	0.027	
70	2.28	0.19	1.71	0.14	1.29	0.13	0.739	0.064	0.407	0.040	0.157	0.013	
80	1.79	0.16	1.42	0.12	0.98	0.10	0.563	0.047	0.319	0.028	0.104	0.012	
90	1.63	0.13	1.26	0.12	0.81	0.07	0.521	0.045	0.231	0.021	0.102	0.010	
100	1.79	0.15	1.26	0.12	0.91	0.08	0.511	0.050	0.204	0.021	0.148	0.022	
110	2.01	0.17	1.36	0.13	0.91	0.08	0.548	0.048	0.215	0.020	0.147	0.024	
120	2.16	0.19	1.40	0.12	1.05	0.09	0.670	0.059	0.306	0.036	0.156	0.016	
125	2.43	0.24											
129													
130			1.56	0.15	1.11	0.09	0.768	0.076	0.412	0.042	0.201	0.023	
ICS	46.3	4.3	39.6	5.2	39.4	4.1	33.9	4.9	23.7	4.5	13.7	1.8	
MTCS	27.7	2.5	22.3	2.9	14.4	1.4	10.1	1.0	5.61	0.86	3.01	0.61	

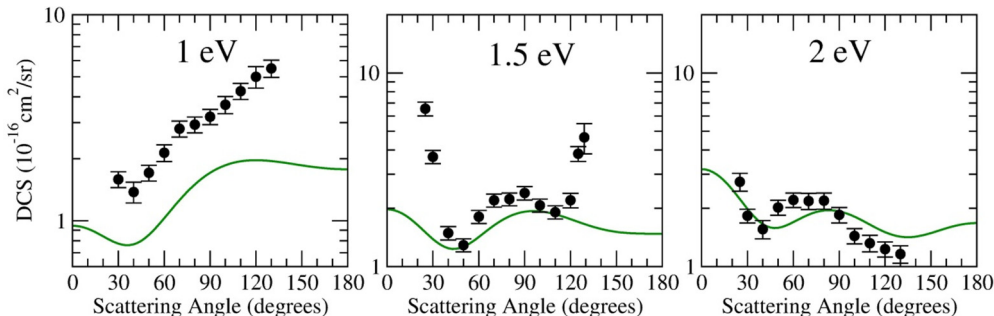


FIG. 4. (Color online) Differential cross sections for elastic scattering of electrons by pentane at 1, 1.5, and 2 eV. We present results in the SEP approximation and compare with the experimental data for pentane. Legend is the same as Fig. 2.

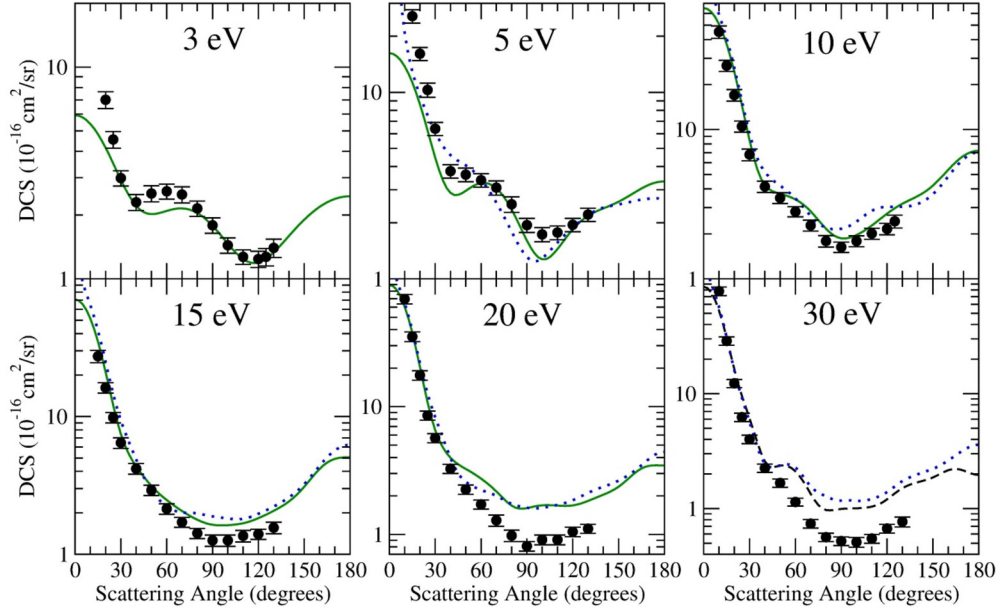


FIG. 5. (Color online) Differential cross sections for elastic scattering of electrons by pentane at 3, 5, 10, 15, 20, and 30 eV. We present results in SEP approximation. We compare our DCS with calculated DCS for *n*-pentanol [37]. Legend is the same as Fig. 2.

where the  $\{|\chi_m\rangle\}$  represents a basis set of  $(N + 1)$ -electron symmetry-adapted Slater determinants, also referred to as configuration-state functions (CSFs). The CSFs are built from products of target states with single-particle wave functions. For the calculations carried out in the static-exchange (SE) approximation, the  $(N + 1)$ -electron basis set (direct space) is given by

$$|\chi_m\rangle = \mathcal{A}(|\Phi_1\rangle \otimes |\phi_m\rangle), \quad (2)$$

where  $|\Phi_1\rangle$  is the target ground state,  $|\phi_m\rangle$  is a single-particle function, and  $\mathcal{A}$  is the antisymmetrizing operator. For the calculations carried out in the static-exchange plus polarization (SEP) approximation, the direct space is augmented by CSFs constructed as

$$|\chi_m\rangle = \mathcal{A}(|\Phi_r\rangle \otimes |\phi_s\rangle), \quad (3)$$

where  $|\Phi_r\rangle$  are  $N$ -electron Slater states obtained by performing single excitations of the target from the occupied (hole) orbitals

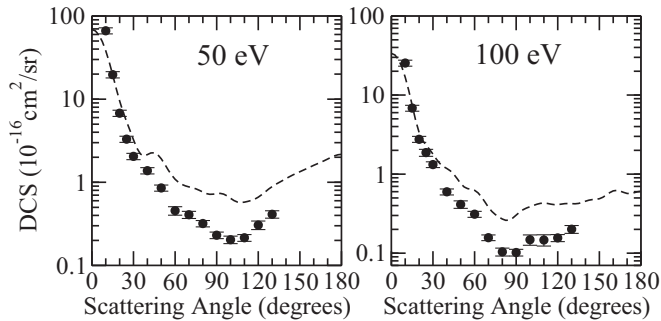


FIG. 6. Differential cross sections for elastic scattering of electrons by pentane at 50 and 100 eV. We present results in the SE (- - -) approximation and compare with present experimental data ( $\bullet$ ).

to a set of unoccupied (particle) orbitals. Here  $|\phi_s\rangle$  is also a single-particle function.

In Eq. (1), the  $d_{mn}$  matrix elements are given by

$$d_{mn} = \langle \chi_m | A^{(+)} | \chi_n \rangle, \quad (4)$$

and the  $A^{(+)}$  operator is given by

$$A^{(+)} = \frac{1}{2}(PV + VP) - VG_P^{(+)}V + \frac{\hat{H}}{N+1} - \frac{1}{2}(\hat{H}P + P\hat{H}). \quad (5)$$

In the above equations  $S_{i(f)}$  is a product of a target state and a plane wave with momentum  $\vec{k}_{i(f)}$ , which is an eigenstate of

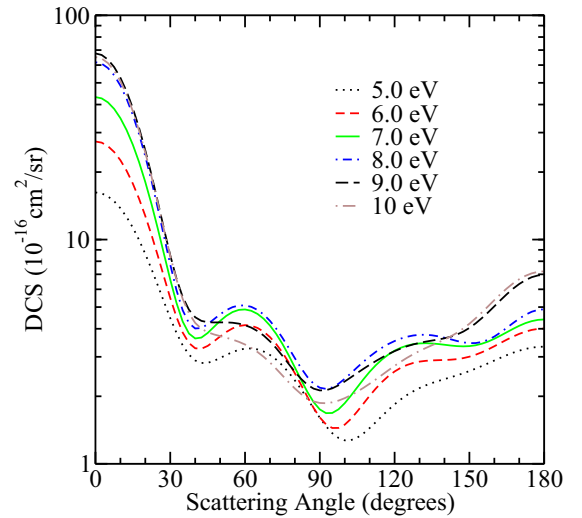


FIG. 7. (Color online) Differential cross sections for elastic scattering of electrons by pentane from 5 to 10 eV showing the *f*-wave distributions at these energies.

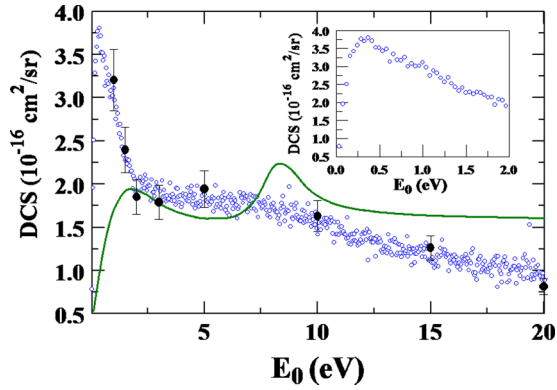


FIG. 8. (Color online) Differential cross sections for elastic scattering of electrons by pentane at  $\theta = 90^\circ$  as a function of  $E_0$ . Legend:  $\circ$  Experiment at  $\theta = 90^\circ$  as a function of  $E_0$ ; — SEP DCSs;  $\bullet$  normalized experimental DCSs at  $\theta = 90^\circ$  from Table I. The inset shows the experimental DCSs for  $E_0 \leq 2$  eV. See text.

the unperturbed Hamiltonian  $H_0$ ;  $V$  is the interaction potential between the incident electron and the target;  $\hat{H} \equiv E - H$  is the collision energy minus the full Hamiltonian of the system, with  $H = H_0 + V$ ;  $P$  is a projection operator onto the open-channel space and  $G_p^{(+)}$  is the free-particle Green's function projected on the  $P$  space.

Our scattering calculations were carried out in the optimized geometry of pentane, which belongs to the  $C_{2v}$  symmetry group. In order to optimize the pentane ground-state geometry we employed the density functional theory (DFT) with the hybrid three-parameter Becke-Lee-Yang-Parr (B3LYP) functional and the DZV +  $+(2d, p)$  basis set, as implemented in the package GAMESS [31]. Figure 1 shows a diagram of the geometrical structure of the molecule.

We used the pseudopotentials of Bachelet *et al.* [32] to replace the core electrons of the carbon atoms and the valence electrons are represented by Cartesian Gaussian functions which were generated according to [33]. The Cartesian Gaussian basis sets used in the present calculations are given elsewhere [26,34]. For hydrogen, we used the  $4s/3s$  basis set of Dunning [35] augmented by one  $p$ -type function with exponent 0.75. The symmetric combinations of the  $d$ -type orbital were excluded to avoid linear dependency in the basis set.

To represent the particle and scattering orbitals we employed modified virtual orbitals (MVOs) [36], which were generated by diagonalizing a cationic Fock operator with charge +6. The SEP space was formed by singlet- and triplet-coupled single-particle excitations from all valence occupied orbitals to the 60 lowest-energy MVOs. We also employed these 60 MVOs as scattering orbitals and obtained 14 998 CSFs for  $A_1$  symmetry, 14 923 CSFs for  $B_2$  symmetry, 13 991 CSFs for  $B_1$  symmetry, and 13 919 CSFs for  $A_2$  symmetry.

### III. RESULTS AND DISCUSSION

#### A. Pentane

The DCSs measured in this work and the ICSs and MTCSs determined from them are presented in Table I. In Fig. 2 we present our calculated integral cross section (ICS), in the SEP approximation, for energies up to 20 eV. We also present in

this figure experimental elastic ICS for electron scattering by pentane. We compare our results with experimental total cross section (TCS) from [15] for electron collision with pentane and calculated data for elastic electron collision with  $n$ -pentanol obtained with the SEP approximation [37]. The alcohol,  $n$ -pentanol, is obtained from pentane by the replacement of a hydrogen in the first carbon by a OH group. One can notice a large difference between pentane and  $n$ -pentanol ICS for low energies, due to the permanent dipole moment present in the  $n$ -pentanol alcohol (1.63 D), while the pentane molecule has a very small (presently calculated) dipole moment (0.08 D). We find good agreement between our calculated data with experimental TCS data [15], mainly in the structure position at 8.5 eV. Agreement between the present experimental elastic ICSs and the TCSs of [15] is good below  $E_0 = 5$  eV except that the rapid rise in the ICSs below 2 eV is not observed in the TCSs. The disagreement at 10 eV between our experimental and calculated ICSs and the TCSs can be understood to be due to the inclusion of inelastic channels. Above 10 eV the opening up of inelastic and ionization channels is consequently responsible for the observed differences between the experimental ICSs and TCSs of this SEP approximation and [38].

In order to characterize the theoretical ICS energy dependence, we show in Fig. 3 the symmetry decomposition of the ICS, according to the  $C_{2v}$  point group. In particular, the broad structure in the SEP ICS at around  $E_0 = 8.5$  eV, presented in Fig. 2, can be explained as due to the overlap of structures belonging to all symmetries and located at around 8 eV in the symmetries  $A_1$  and  $A_2$ , and at around 9 eV in the symmetries  $B_1$  and  $B_2$ .

In Figs. 4–6 we present our calculated differential cross sections (DCSs) at selected energies between 1 and 100 eV. For energies up to 20 eV we present results in the SEP approximation and for higher energies we present results in the SE approximation. We also compare our calculated DCSs with the calculated DCS for  $n$ -pentanol [37] and with experimental DCSs for pentane. In Fig. 4, at our lowest  $E_0$  values of 1 and 1.5 eV, the experimental DCSs show rapid change in angular behavior from strongly backward scattering at  $E_0 = 1$  eV to a  $d$ -type angular distribution at  $E_0 = 1.5$  eV, which is not observed in the SEP results, although this picture improves at  $E_0 = 2$  eV, showing forward scattering typically due to the static dipole polarizability of pentane whose average value is large at  $\approx 9.6 \text{ \AA}^3$  [39]. The low-energy experimental DCSs clearly demonstrate the role of polarizability of pentane at even our lowest  $E_0$  values. Such rapid changes in DCS angular distributions with  $E_0$  at low  $E_0$  values are typical of such alkane targets and have been seen, e.g., in [10,40,41].

For  $E_0$  higher than  $E_0 = 2$  eV we see much-improved agreement with our SEP calculations, and increased forward scattering due to the influence of target polarizability. A prominent secondary maximum around  $\theta = 70^\circ$  first observed at  $E_0 = 1.5$  eV persists up to the ionization energy. At  $E_0 = 5$  to 15 eV, agreement between experiment and the SEP is very good. We also observe that the SEP values from pentanol follow those of pentane, except that the permanent dipole of pentanol produces a somewhat more pronounced forward peak at  $E_0 = 5$  and 10 eV. Above the ionization potential, this is

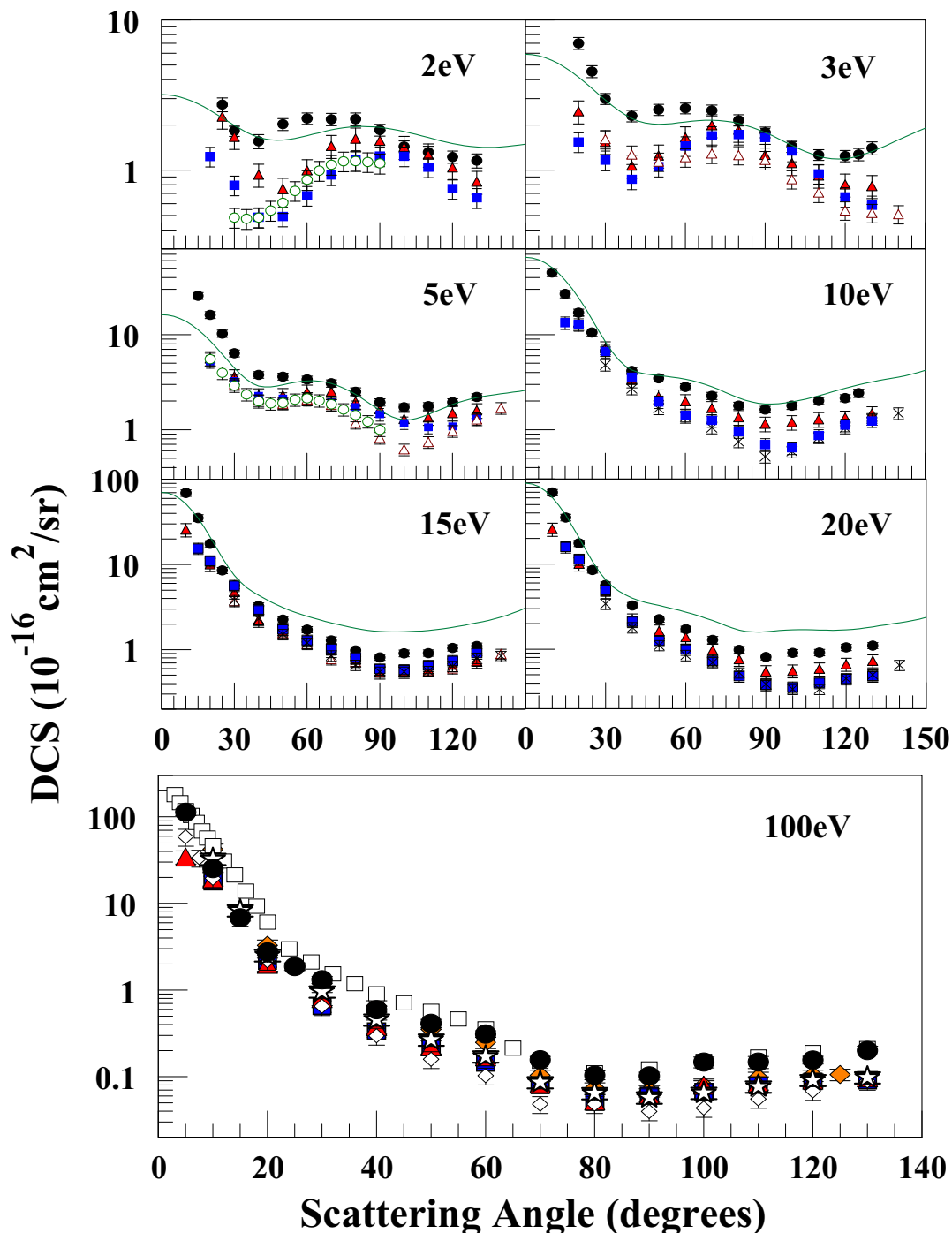


FIG. 9. (Color online) DCSs for elastic scattering of electrons by ethane, propane, butane, and pentane for selected  $E_0$  values. Legend: **Ethane:** ■ Tanaka *et al.* [46]; △ Mapstone and Newell [47], × Curry and Newell [48], ○ Merz and Linder [49], ◇ Rawat *et al.* [9], and □ Fink *et al.* [50]. **Propane:** ▲ Boesten *et al.* [10] and ◆ Souza *et al.* [12]. **Butane:** ☆ Sanches *et al.* [13]. **Pentane:** ● Present experiment and — present calculations. See text for discussion.

no longer the case and the polarizability is more dominant. We observe an  $f$ -wave behavior in the theoretical and experimental DCSs around 10 eV. For higher energies, there are some discrepancies in magnitude between the calculated and the experimental DCSs. This is because our calculations consider only the elastic channel, and there is no flux loss from the elastic channel into the inelastic channels. It has been shown that including the inelastic channels the DCSs move

down toward the experimental data [38,42]. At  $E_0 \geq 20$  eV intermediate to large  $\theta$  agreement between the theory (SE and SEP) is much reduced, as is expected, due to the close-coupling breakdown of the theory not to be able to include the increase in the scattering channels greatly above the ionization energy as shown in Figs. 5 and 6.

In Fig. 7 we show the calculated SEP elastic DCSs for  $E_0$  from 5 to 10 eV in 1-eV steps illustrating the  $f$ -wave

dependence (with DCS minimum at  $\theta = 90^\circ$ ) in angular distribution around the 8-eV resonance energy. A similar behavior is observed in alkanes, alcohols, and amines of straight-chain structures [26,30,37,43–45]. This is in contrast to branched-chain molecules where the  $d$ -type behavior is observed (i.e., a DCS local maximum at  $\theta = 90^\circ$ ).

In Fig. 8 we show our  $\theta = 90^\circ$  DCSs as a function of  $E_0$  from 0.317 to 20 eV (so-called “excitation curve”). Our experimental  $90^\circ$  DCSs (taken at fixed  $E_0$  values vs  $\theta$ , and taken at the fixed  $\theta = 90^\circ$  vs  $E_0$ ) are in good agreement with each other; however, we observe a sharp maximum at about 0.37 eV (see inset in the figure), due to a Feshbach resonance followed by a broader shape resonance feature at around 8.3 eV (due to the symmetry components of Fig. 3) that is observed to be much sharper in the SEP theory than experiment. Both theory and experimental DCSs decrease sharply as  $E_0$  approaches 0 eV, where we can expect a RT minimum as expected for alkanes, e.g., Floriano *et al.* [16], where the minimum is at an  $E_0$  value not possible to access with the present experiment. This type of minimum was also observed in the computed cross sections for alcohols, such as methanol, ethanol,  $n$ -propanol,  $n$ -butanol, and  $n$ -pentanol [37].

### B. Comparison with other linear $n$ -alkanes

Floriano *et al.* [16] noticed from swarm experiments that the RT minimum in the electron momentum-transfer cross section (MTCS) occurs at the same energy ( $\sim 0.12$  eV) in all  $n$ -alkanes from  $C_2H_6$  to  $C_{10}H_{22}$ . Moreover the experiments show [16] that it is the molecular size that determines the magnitude of the MTCS rather than the energy dependence. A weak energy dependence on chain length indicates that the electron being scattered interacts with chain segments that contain only two or three carbon atoms. The longer chain mainly increases the number of scattering centers enhancing the average cross section. Here we notice a similar trend for DCS of  $n$ -alkanes—the length of molecular chain changes more the magnitude of DCS than the shape of its angular dependence for a given  $E_0$ . This general tendency is presented in Fig. 9 where we compare our experimental DCS for pentane ( $C_5H_{12}$ ) with available DCS experimental data for shorter linear alkanes  $C_nH_{2n+2}$  from this family such as ethane ( $C_2H_6$ ), propane ( $C_3H_8$ ), and butane ( $C_4H_{10}$ ). While there are low and intermediate  $E_0$  ( $< 50$  eV) elastic DCSs for ethane and propane, only intermediate  $E_0$  ( $> 50$  eV) DCSs exist for butane [13].

At  $E_0 = 2$  and 3 eV, the experimental DCS data display similar angular distributions with a forward (polarizability) peaking followed by a minimum at around  $\theta = 40^\circ - 50^\circ$  and a maximum around  $80^\circ$ . At higher energies the shapes are identical except that the ethane and propane DCSs are generally (and expectedly) lower in magnitude than present results for pentane. The very early DCSs of Fink *et al.* [50]

likely suffer from normalization effects and are of somewhat different angular behavior compared to most other DCSs. In particular, the DCS data for propane [10] are lower by a factor of  $\approx 0.76$ , which roughly reflects the ratio of chain lengths. At  $E_0 = 100$  eV, where we can also compare to butane DCSs we see butane’s DCS range in between pentane and propane, as expected, being lower than pentane by a factor of  $\approx 0.88$ , allowing for experimental uncertainties. At small  $\theta$ , our DCSs are lower than some data for other alkanes which we attribute to problems in background evaluation from the other experiments as compared to the present where our movable source arrangement is expected to produce a better characterization of the background.

## IV. CONCLUSION

We have presented theoretical and experimental differential elastic scattering cross sections for pentane using the Schwinger multichannel method with pseudopotentials and the aperture target, movable source method, over a wide range of  $E_0$  and  $\theta$  values. Overall agreement between theory and experiment is good at between  $3 \text{ eV} \leq E_0 \leq 15 \text{ eV}$ , which is typical of SMC calculations. The differential cross sections at around 10 eV, where pentane displays a broad structure in the integral cross section, has a typical  $f$ -wave oscillatory behavior, which has already been observed in  $n$ -alkanes, alcohols, and amines with linear chains. In addition we notice that (discounting the very early DCSs of Fink *et al.* [50] which very likely suffer from normalization effects) the magnitude of pentane DCSs are slightly higher, while their angular dependence is similar, when compared to experimental data reported for shorter linear  $n$ -alkanes in a wide  $E_0$  range between 1 and 100 eV.

## ACKNOWLEDGMENTS

K.F. acknowledges the Fulbright Program for a fellowship to conduct this work at California State University Fullerton. M.A.K. and L.R.H. acknowledge support from National Science Foundation research grants (Grants NSF-RUI-AMO No. 1306742 and No. 0968874). A.S.B. acknowledges support from Brazilian Agency Coordenação de Aperfeiçoamento de Pessoal de Nível Superior (CAPES). M.H.F.B. acknowledges support from Brazilian agencies Conselho Nacional de Desenvolvimento Científico e Tecnológico (CNPq), and FINEP (under project CTInfra). A.S.B. and M.H.F.B. also acknowledge computational support from Professor Carlos M. de Carvalho at LFTC-DFis-UFPR and at LCPAD-UFPR, and from CENAPAD-SP. We acknowledge Professor Vincent McKoy and Dr. Carl Winstead for fruitful discussions and for useful input regarding this manuscript.

- 
- [1] R. Minetti, M. Ribaucour, M. Carlier, C. Fittschen, and L. R. Sochet, *Combust. Flame* **96**, 201 (1994).  
 [2] S. Kojima, *Combust. Flame* **99**, 87 (1994).  
 [3] C. Q. Jiao, C. A. DeJoseph, Jr., and A. Garscadden, *J. Phys. D: Appl. Phys.* **40**, 409 (2007).

- [4] S. Bhattacharjee, S. Paul, and S. Ghosh, *Phys. Plasmas* **21**, 082103 (2014).  
 [5] H. Cho, Y. S. Park, E. A. y Castro, G. L. Souza, I. Iga, L. E. Machado, L. M. Bescansin, and M.-T. Lee, *J. Phys. B: At. Mol. Phys.* **41**, 045203 (2008).

- [6] T. Nishimura and F. A. Gianturco, *J. Phys. B: At. Mol. Phys.* **35**, 2873 (2002).
- [7] R. Čurík, P. Čársky, and M. Allan, *J. Phys. B: At. Mol. Opt. Phys.* **41**15203 (2008).
- [8] M. H. F. Bettega, R. F. da Costa, and M. A. P. Lima, *Braz. J. Phys.* **39**, 69 (2009).
- [9] P. Rawat, M. G. P. Homem, R. T. Sugohara, I. P. Sanches, I. Iga, G. L. C. de Souza, A. S. dos Santos, R. R. Lucchese, L. E. Machado, L. M. Bescansin, and M.-T. Lee, *J. Phys. B: At. Mol. Opt. Phys.* **43**, 225202 (2010).
- [10] L. Boesten, M. A. Dillon, H. Tanaka, M. Kimura, and H. Sato, *J. Phys. B* **27**, 1845 (1994).
- [11] D. B. Popović, D. E. David, J. Michl, P. Čurík, and P. Čársky, *J. Chem. Phys.* **121**, 10551 (2004).
- [12] G. L. C. de Souza, M.-T. Lee, I. P. Sanches, P. Rawat, I. Iga, A. S. dos Santos, L. E. Machado, R. T. Sugohara, L. M. Bescansin, M. G. P. Homem, and R. R. Lucchese, *Phys. Rev. A* **82**, 012709 (2010).
- [13] I. P. Sanches, R. T. Sugohara, L. Rosani, M.-T. Lee, and I. Iga, *J. Phys. B: At. Mol. Opt. Phys.* **41**, 185202 (2008).
- [14] G. R. Freeman, I. György, and S. S.-S. Huang, *Can. J. Chem.* **57**, 2626 (1979).
- [15] M. Kimura, O. Sueoka, A. Hamada, and Y. Itikawa, *Adv. Chem. Phys.* **111**, 537 (2000).
- [16] M. A. Floriano, N. Gee, and G. R. Freeman, *J. Chem. Phys.* **84**, 6799 (1986).
- [17] B. Boudaïffa, P. Cloutier, D. Hunting, M. A. Huels, and L. Sanche, *Science* **287**, 1658 (2000).
- [18] M. A. Khakoo, C. E. Beckmann, S. Trajmar, and G. Csanak, *J. Phys. B* **27**, 3159 (1994).
- [19] K. Takatsuka and V. McKoy, *Phys. Rev. A* **24**, 2473 (1981); **30**, 1734 (1984).
- [20] M. A. P. Lima, L. M. Bescansin, A. J. R. da Silva, C. Winstead, and V. McKoy, *Phys. Rev. A* **41**, 327 (1990).
- [21] M. H. F. Bettega, L. G. Ferreira, and M. A. P. Lima, *Phys. Rev. A* **47**, 1111 (1993).
- [22] J. C. Traeger, C. E. Hudson, and D. J. McAdoo, *J. Am. Soc. Mass Spectrom.* **7**, 73 (1996).
- [23] ARi Industries Inc., Addison, IL60101 USA, 1HN040B-16.3 biaxial cable.
- [24] ETP Equipe Thermodynamique et Plasmas (ETP) model AF151.
- [25] J. H. Brunt, G. C. King, and F. H. Read, *J. Phys. B: At. Mol. Phys.* **10**, 1289 (1977).
- [26] M. A. Khakoo, J. Muse, H. Silva, M. C. A. Lopes, C. Winstead, V. McKoy, E. M. de Oliveira, R. F. da Costa, M. T. do N. Varella, M. H. F. Bettega, and M. A. P. Lima, *Phys. Rev. A* **78**, 062714 (2008).
- [27] M. Hughes, K. E. James, Jr., J. G. Childers, and M. A. Khakoo, *Meas. Sci. Technol.* **14**, 841 (1994).
- [28] R. K. Nesbet, *Phys. Rev. A* **20**, 58 (1979).
- [29] D. F. Register, S. Trajmar, and S. K. Srivastava, *Phys. Rev. A* **21**, 1134 (1980).
- [30] K. Fedus, C. Navarro, L. R. Hargreaves, M. A. Khakoo, F. M. Silva, M. H. F. Bettega, C. Winstead, and V. McKoy, *Phys. Rev. A* **90**, 032708 (2014).
- [31] M. W. Schmidt, K. K. Baldrige, J. A. Boatz, S. T. Elbert, M. S. Gordon, J. H. Jensen, S. Koseki, N. Matsunaga, K. A. Nguyen, S. J. Su, T. L. Windus, M. Dupuis, and J. A. Montgomery, *J. Comput. Chem.* **14**, 1347 (1993).
- [32] G. B. Bachelet, D. R. Hamann, and M. Schlüter, *Phys. Rev. B* **26**, 4199 (1982).
- [33] M. H. F. Bettega, A. P. P. Natalense, M. A. P. Lima, and L. G. Ferreira, *Int. J. Quantum Chem.* **60**, 821 (1996).
- [34] M. A. Khakoo, J. Blumer, K. Keane, C. Campbell, H. Silva, M. C. A. Lopes, C. Winstead, V. McKoy, R. F. da Costa, L. G. Ferreira, M. A. P. Lima, and M. H. F. Bettega, *Phys. Rev. A* **77**, 042705 (2008).
- [35] T. H. Dunning, Jr., *J. Chem. Phys.* **53**, 2823 (1970).
- [36] C. W. Bauschlicher, Jr., *J. Chem. Phys.* **72**, 880 (1980).
- [37] E. M. de Oliveira, M. T. do N. Varella, M. H. F. Bettega, and M. A. P. Lima, *Eur. Phys. J. D* **68**, 65 (2014).
- [38] R. F. da Costa, M. H. F. Bettega, M. A. P. Lima, M. C. A. Lopes, L. R. Hargreaves, G. Serna, and M. A. Khakoo, *Phys. Rev. A* **85**, 062706 (2012).
- [39] NIST Computational Chemistry Comparison and Benchmark Database, NIST Standard Reference Database No. 101, Release 16a, August 2013, edited by Russell D. Johnson III; available at <http://cccbdb.nist.gov/polcalccomp2.asp?method=3&basis=4>.
- [40] R. Merz and F. Linder, *J. Phys. B* **36**, 2921 (2003).
- [41] W. Sohn, K. Jung, and H. Ehrhardt, *J. Phys. B* **16**, 891 (1983).
- [42] R. F. da Costa, M. H. F. Bettega, M. T. do N. Varella, E. M. de Oliveira, and M. A. P. Lima, *Phys. Rev. A* **90**, 052707 (2014).
- [43] M. H. F. Bettega, R. F. da Costa, and M. A. P. Lima, *Phys. Rev. A* **77**, 052706 (2008).
- [44] A. R. Lopes, M. H. F. Bettega, M. A. P. Lima, and L. G. Ferreira, *J. Phys. B* **37**, 997 (2004).
- [45] M. H. F. Bettega, M. A. P. Lima, and L. G. Ferreira, *J. Phys. B* **40**, 3015 (2007).
- [46] H. Tanaka, L. Boesten, D. Matsunaga, and T. Kudo, *J. Phys. B* **21**, 1255 (1988).
- [47] B. Mapstone and W. R. Newell, *J. Phys. B* **25**, 491 (1992).
- [48] P. J. Curry, W. R. Newell, and A. C. H. Smith, *J. Phys. B* **18**, 2303 (1985).
- [49] R. Merz and F. Linder, *J. Phys. B* **31**, 4663 (1998).
- [50] M. Fink, K. Jost, and D. Hermann, *J. Chem. Phys.* **63**, 1985 (1975).